SCIENTIFIC REPORTS
nature research

OPEN

Active control on topological immunity of elastic wave metamaterials

Guan-Hua Li[1], Tian-Xue Ma[2], Yi-Ze Wang[3] ✉ & Yue-Sheng Wang[1,3]

The topology concept in the condensed physics and acoustics is introduced into the elastic wave metamaterial plate, which can show the topological property of the flexural wave. The elastic wave metamaterial plate consists of the hexagonal array which is connected by the piezoelectric shunting circuits. The Dirac point is found by adjusting the size of the unit cell and numerical simulations are illustrated to show the topological immunity. Then the closing and breaking of the Dirac point can be generated by the negative capacitance circuits. These investigations denote that the topological immunity can be achieved for flexural wave in mechanical metamaterial plate. The experiments with the active control action are finally carried out to support the numerical design.

Phononic crystals and elastic wave metamaterials are artificial structures which are arranged periodically and have received lots of attention[1–8]. These new kinds of structures have many extraordinary properties, e.g. the wave band gaps[9–12], negative refraction[13,14], acoustic/elastic wave cloaks[15–17], etc. These interesting behaviors can be used to tune the wave propagation properties and have a wide variety of potential engineering applications. Acoustic couplers[18], sensors[19] and waveguides[20] are several typical applications of phononic crystals and elastic wave metamaterials.

In recent years, a lot of attention has been focused on the extraordinary transmission phenomena of acoustic/elastic waves near the Dirac point. The periodic structures with the Dirac point can present many interesting behaviors, e.g. carrier mobility[21], zero refractive index[22–25], Hall effect[26] and topological edge states[27–30], etc. It should be mentioned that in the photonic crystal, the spatial phase can be reconstructed by the degenerate Bloch modes at the Dirac point[31]. Moreover, the topological phase can also transform because of the band inversion[32].

On the other hand, some investigations have been reported on the phononic crystals and elastic wave metamaterials with the active control action[33–37]. To present the controllable flexural waves with the broadband characteristics by the active control, an experiment using the shunted piezoelectric patches was reported[38]. Furthermore, another experiment was performed to show the tunable waveguide of the phononic plate[39]. Although the active control action has been applied on the waveguide structures, its tunable effects on the topological properties of elastic wave metamaterials have not been considered. In this work, we propose a tunable topological state of the flexural wave with the active control. Based on the electrical control action, the Dirac point and its corresponding topological immunity can be achieved.

Methods

In this work, we focus on elastic wave metamaterials with double Dirac points locating at the center of the Brillouin zone. A hexagonal unit cell in the elastic wave metamaterial plate is showed in Fig. 1(a). The cell is made of the resin and its six corners are attached with the piezoelectric material P-4 on both sides. The parameters are illustrated in Table 1, where a is the lattice constant, R is the radius of the piezoelectric patch, h_1–h_3 are the thicknesses of the middle layer, groove and piezoelectric sheet, respectively. Each piezoelectric patch is connected by a negative capacitance circuit to behave as the active control load in Fig. 1(b). As shown in Fig. 1(c), the negative capacitance circuit is used in the active control system to change the elastic modules, in which the capacitance C_p, compensation resistance R_0, operational amplifier, fixed resistances R_1 and sliding rheostat R_2 are considered. The derivation of the negative capacitance circuit is presented in

[1]Institute of Engineering Mechanics, Beijing Jiaotong University, Beijing, 100044, China. [2]Department of Civil Engineering, University of Siegen, Siegen, D-57068, Germany. [3]Department of Mechanics, Tianjin University, Tianjin, 300350, China. ✉e-mail: wangyize@tju.edu.cn

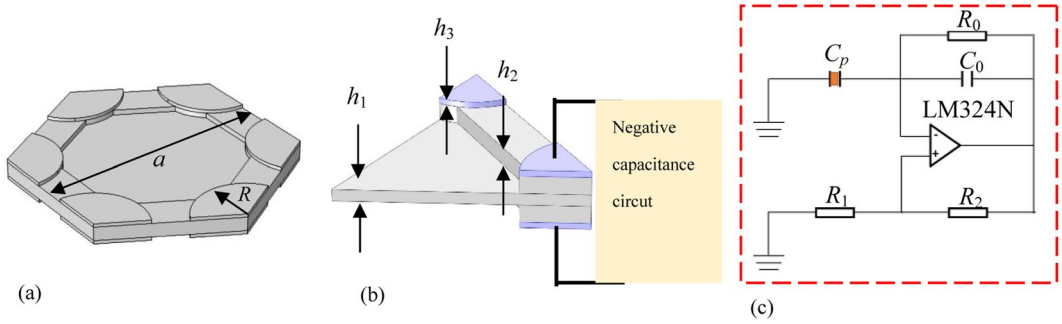

Figure 1. (**a**) A unit cell bonded by piezoelectric patches, (**b**) the piezoelectric patches attached by the negative capacitance circuits and (**c**) the negative capacitance circuit.

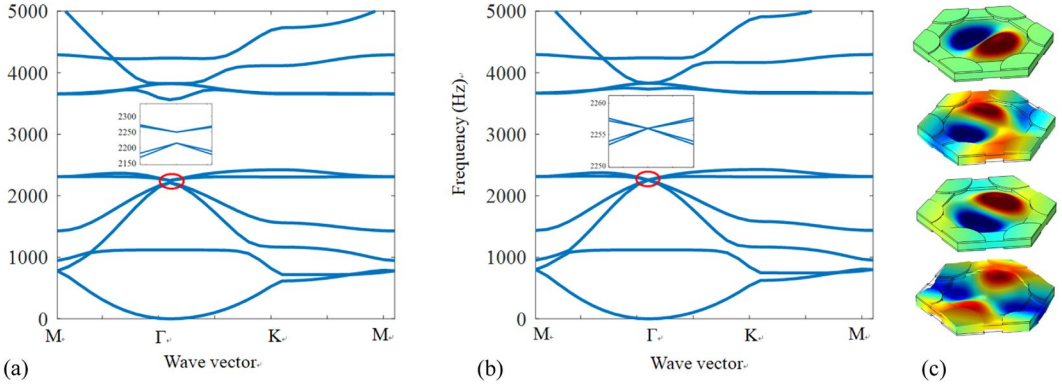

Figure 2. (**a**) Band gap, (**b**) the Dirac point induced by the electric circuit and (**c**) its displacement fields of the four degenerate states at the Dirac point.

a (mm)	h_1 (mm)	h_2 (mm)	h_3 (mm)	h_4 (mm)
$40\sqrt{3}$	1	1.554	1	15

Table 1. The parameters of the unit cell.

Supplementary Material. Both the dispersion curves and propagation properties are calculated by the finite element software COMSOL. Our attention is focused on the topological immunity of the elastic wave in which the energy bands of the flexural modes are presented.

Results and discussions

When the negative capacitance circuits are not connected, the band structure calculated by the finite element method is shown in Fig. 2(a) and we can see that the band gap width is about 35 Hz. In order to generate the Dirac point, the negative capacitance circuits are connected and the parameter of the resistance $\alpha = 0.9$ in Eq.(A.4) is applied. The band structure with the Dirac point is shown in Fig. 2(b), in which a quadruple degeneracy at 2256 Hz can be observed. The displacement field distributions for the four degenerate states at the Dirac point are presented in Fig. 2(c).

An interesting behavior is the extraordinary transmission at the Dirac cone. In this work, it is designed by the configuration and electrical tuning to show the immune property of the elastic wave to the object. Then the concept "topological immunity" is applied to present the propagation of the flexural wave around the circular defect. This phenomenon makes the active controllable structure can immunize to the object, which means that the metamaterial plate exhibits a robust property at a certain frequency. Then, we can design an elastic wave metamaterial plate as a new function to achieve the topological immunity of the flexural wave. This work demonstrates the similar physics to ref. [40] for elastic wave and an additional tuning approach. Due to both the P-symmetry and T-symmetry can be found, the Berry curvature and Chern number are zero. The periodic structure is excited by a shaker at the right boundary and the frequency response is considered.

Here we define the transmission coefficient as the ratio of the left to the right flexural displacements. From the transmission coefficient curve for the elastic wave metamaterial plate with a defect in Fig. 3(a), a peak with 0.91 at the frequency of 2377.9 Hz is found. At this frequency, the flexural waves are almost

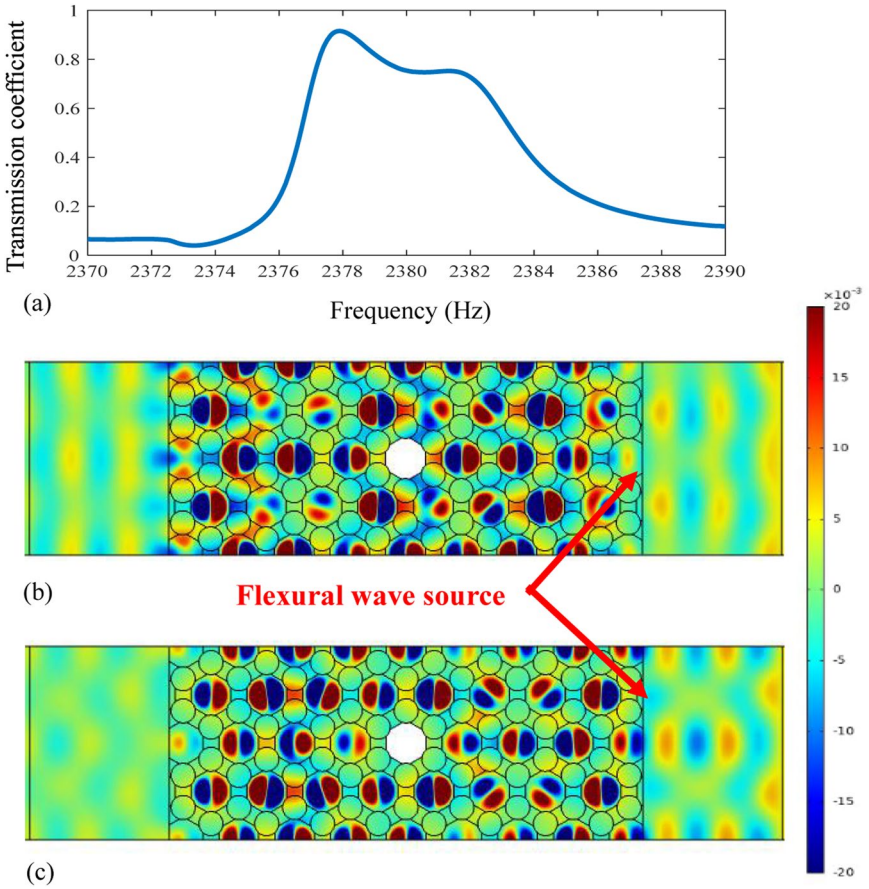

Figure 3. (**a**) Transmission coefficient, (**b**) wave propagation at 2377.9Hz with electrical circuits and (**c**) wave propagation without electrical circuits at 2377.9 Hz.

Material	Mass density ρ (kg/m^3)	Young's modulus E (N/m^2)	Compliance coefficient s_{11}^E (m^{3}N^{-1})	Piezoelectric strain coefficient d_{31} (Cm^{-2})	Permittivity ε_{33}^T (Fm^{-1})
P-4	7450	8.83×10^{10}	1.2×10^{-11}	-1×10^{-10}	-1×10^{-10}

Table 2. The material parameters of the piezoelectric patch.

perfectly transmitted through the whole system. Furthermore, when the frequency of the incident wave is 2377.9 Hz which is close to the Dirac point, the phase change becomes almost invisible in Fig. 3(b). Although there is a weak reflection on the right side, the defect is undetectable from the left field. Generally speaking, 2377 Hz does not shift obviously compared to 2256 Hz. It is mainly because of the problems during the mesh generation and boundary condition setting. An important influence is that the band structure is calculated with the infinite periodic boundary condition but the transmission spectrum is calculated with finite periodic structures.

In order to support these numerical results, the transmission response of the metamaterial plate without external circuits is calculated and shown in Fig. 3(c). We can see that the transmission becomes low and the waveform is observably distorted, which means that the topological immunity is achieved by the active control. The tunable effects of the active control on the topological immunity are considered, in which the negative capacitance circuits are applied to generate the Dirac point. When the Dirac point appears in the band structure, the topological immunity in the elastic wave metamaterial plate can be found. At the same time, there is only one peak in the transmission coefficient curve, which corresponds to the Dirac point.

Then, the active control experiments are performed on the elastic wave metamaterial plate in which the P-4 piezoelectric patches are boned at the corners. The elastic wave metamaterial plate is fabricated by the 3D printing technology with 8000 synthetic resin, in which the Young's modulus $E = 2.5$ GPa, density $\rho = 1300$ kg/m^3 and Poisson's ratio $\nu = 0.41$. The material parameters of the P-4 piezoelectric patch are shown in Table2 and the operational amplifier LM324N is applied.

The experimental setup is illustrated in Fig. 4(a), in which the elastic wave metamaterial plate is connected by the negative capacitance circuits. The exciter and the four received points e–h are illustrated in Fig. 4(b). The plate

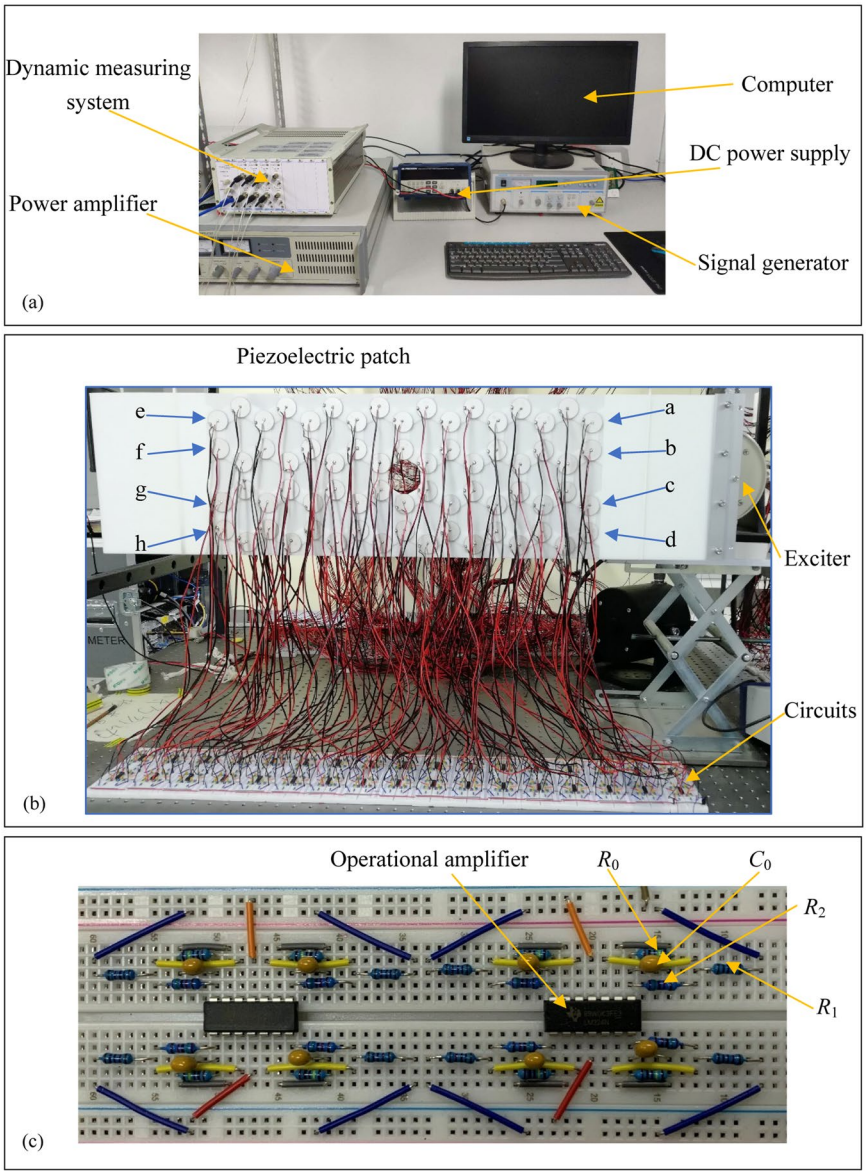

Figure 4. Experimental setup: (**a**) The testing system, (**b**) the whole structure with the active control system and (**c**) the negative capacitance circuit.

C (pF)	C_p (pF)	R_2 (kΩ)	R_1 (kΩ)	R_0 (kΩ)	Operational amplifier
9.684	8.155	51.54	68	2000	LM324N

Table 3. The parameters of the negative capacitance circuit.

and exciter are connected by a fixture with a high rigidity to generate the flexural wave. During the experiment, 4×9 unit cells are applied to the elastic wave metamaterial plate and the sample size in Fig. 4(b) is same as that in Fig. 3(b). On the other hand, the power supply depends on the operational amplifier which is shown in Fig. 4(c). The description of the circuit is listed in Table 3. Due to the limitation of experimental conditions, only the finite periodic structures can be used for to support the numerical simulation. Although there is a little difference between the experimental and the numerical results, similar topological immune phenomenon can also be found during the experiment.

Figures 5 and 6 show the experimental results, in which the solid lines correspond to the points a–d (wave source) and dotted lines represent points e–h (response). With the connecting circuits on the elastic wave metamaterial plate in Fig. 5, we can see that although there is a little difference between the exciting and receiving points, their responses are quite similar at 2247 Hz. According to both numerical and experimental results, the waveform keeps the same from the right to the left sides. It means that the topological immunity is realized by the

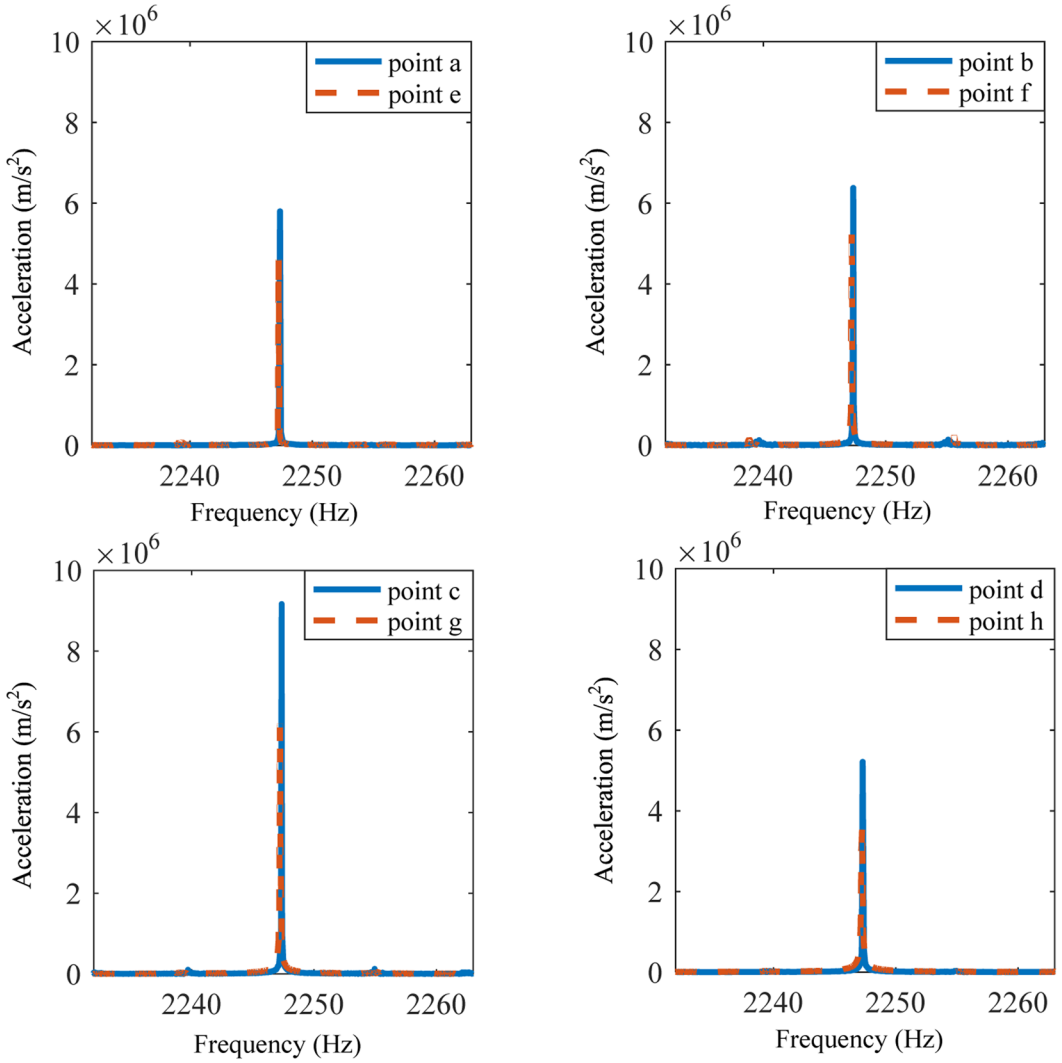

Figure 5. Responses of points a-h at 2247 Hz when the elastic wave metamaterial plate is attached by the active control system.

active control action. Then, the experiment is performed for the periodic structure without active control systems at the same frequency. As shown in Fig. 6, we can obviously see that the responses of the points e–h are quite smaller than those of the points a–d. It denotes that the flexural wave signal cannot be received on the left side for the structure without the active control.

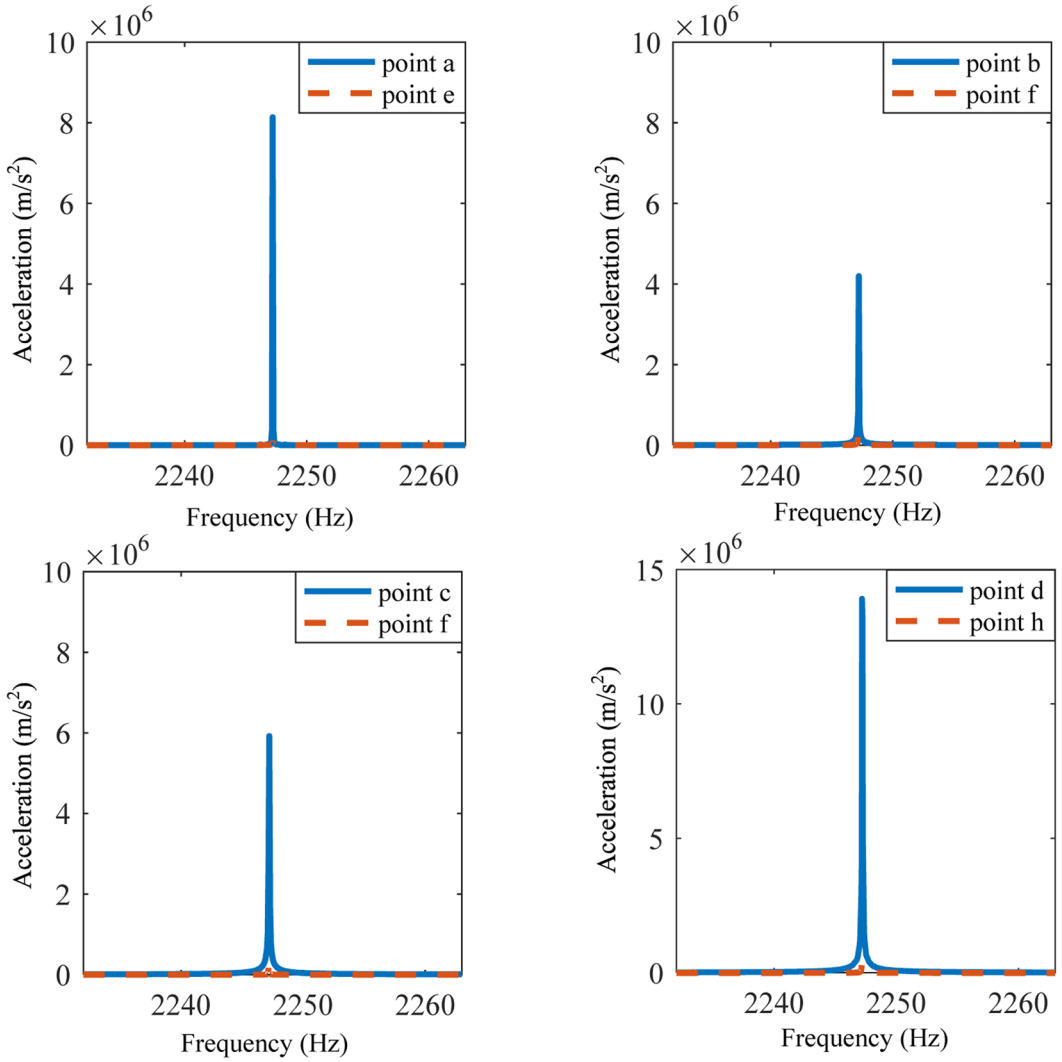

Figure 6. Responses of points a-h at frequency at 2247Hz when the elastic wave metamaterial plate is not attached by the active control system.

Conclusions

In this work, an elastic wave metamaterial plate with the active control system is design to illustrate the topological immune property. The band structure is calculated by the numerical simulation and the double Dirac point is achieved by the external negative capacitance circuits. Around the Dirac point, the transmission responses of the metamaterial plate with a defect are discussed. Experiments are performed with the 3D printing metamaterial plate being bonded by the external electrical circuits. The topological immunity is observed by the responses behind the defect and achieved by the control action.

Received: 6 January 2020; Accepted: 13 May 2020;
Published online: 10 June 2020

References

1. Krodel, S. & Delpero, T. 3D auxetic microlattices with independently controllable acoustic band gaps and quasi-static elastic moduli. *Advanced Engineering Materials* **4**, 357–363 (2014).
2. Qureshi, A., Li, B. & Tan, K. T. Numerical investigation of band gaps in 3D printed cantilever-in-mass metamaterials. *Scientific Reports* **6**, 28314 (2016).
3. Li, B., Alamri, S. & Tan, K. T. A diatomic elastic metamaterial for tunable asymmetric wave transmission in multiple frequency bands. *Scientific Reports* **7**, 6226 (2017).
4. Li, X., Chen, Y., Hu, G. & Huang, G. A self-adaptive metamaterial beam with digitally controlled resonators for subwavelength broadband flexural wave attenuation. *Smart Materials and Structures* **27**, 045015 (2018).
5. Zhang, Y. F., Li, B., Zheng, Q. S., Genin, G. M. & Chen, C. Q. Programmable and robust static topological solitons in mechanical metamaterials. *Nature Communications* **10**, 5605 (2019).
6. Park, H. W. & Oh, J. H. Study of abnormal group velocities in flexural metamaterials. *Scientific Reports* **9**, 1–13 (2019).
7. Elmadih, W. *et al*. Three-dimensional resonating metamaterials for low-frequency vibration attenuation. *Scientific Reports* **9**, 11503 (2019).
8. Li, S. B. *et al*. Designing a broad locally-resonant bandgap in a phononic crystals. *Physics Letters A* **382**, 1371–1377 (2019).

9. Wu, Z. J., Li, F. M. & Zhang, C. Z. Vibration band-gap properties of three-dimensional Kagome lattices using the spectral element method. *Journal of Sound and Vibration* **341**, 162–173 (2015).
10. Dong, H. W., Wang, Y. S. & Zhang, C. Z. Topology optimization of chiral phoxonic crystals with simultaneously large phononic and photonic bandgaps. *IEEE Photonics Journal* **9**, 19430655 (2017).
11. He, J. H. & Huang, H. H. Complete vibrational bandgap in thin elastic metamaterial plates with periodically slot-embedded local resonators. *Archive of Applied Mechanics* **88**, 1263–1274 (2018).
12. Fu, C. Y., Xu, J. X., Zhao, T. F. & Chen, C. Q. A mechanical wave switch with tunable frequency output. *Applied Physics Letters* **115**, 191902 (2019).
13. Croenne, C., Morvan, B., Vasseur, J., Dubus, B. & Hladky-Hennion, A. Analysis of elastic waves transmitted through a 2-D phononic crystal exhibiting negative refraction. *IEEE Transactions on Ultrasonics Ferroelectrics and Frequency Control* **58**, 178–186 (2011).
14. Zhu, R., Liu, X. N., Hu, G. K., Sun, C. T. & Huang, G. L. Negative refraction of elastic waves at the deep-subwavelength scale in a single-phase metamaterial. *Nature Communications* **5**, 5510 (2014).
15. Torrent, D. & Sánchez-Dehesa, J. Acoustic cloaking in two dimensions: a feasible approach. *New Journal of Physics* **10**, 063015 (2008).
16. Zhang, S., Xia, C. & Fang, N. Broadband acoustic cloak for ultrasound waves. *Physical Review Letters* **106**, 024301 (2011).
17. Farhat, M. *et al*. A homogenization route towards square cylindrical acoustic cloaks. *New Journal of Physics* **10**, 115030 (2008).
18. Herrmann, H., Schaefer, K. & Sohler, W. Polarization independent, integrated optical, acoustically tunable wavelength filters/switches with tapered acoustical directional coupler. *IEEE Photonics Technology Letters* **6**, 1335–1337 (1994).
19. Lucklum, R., Zubtsov, M. & Ke, M. Liquid sensor utilizing a regular phononic crystal with normal incidence of sound. *IEEE Transactions on Ultrasonics Ferroelectrics and Frequency Control* **59**, 463–471 (2012).
20. Nishizawa, J. *et al*. THz generation from gap rod-type waveguides. *IEEE Photonics Technology Letters* **19**, 143–145 (2007).
21. Li, F. *et al*. Benzene-like N_6 rings in a Be_2N_6 monolayer: a stable 2D semiconductor with high carrier mobility. *Journal of Materials Chemistry C* **5**, 11515 (2017).
22. Edwards, B., Alu, A., Young, M. E., Silveriinha, M. & Engheta, N. Experimental verification of epsilon-near-zero metamaterial coupling and energy squeezing using a microwave waveguide. *Physical Review Letters* **100**, 033903 (2008).
23. Moitra, P. *et al*. Realization of an all- dielectric zero-index optical metamaterial. *Nature Photonics* **7**, 791–795 (2013).
24. Li, Y. *et al*. On-chip zero-index metamaterials. *Nature Photonics* **9**, 738–742 (2015).
25. Dubois, M., Shi, C., Zhu, X., Wang, Y. & Zhang, X. Observation of acoustic Dirac-like cone and double zero refractive index. *Nature Communications* **8**, 14871 (2017).
26. Hatsugai, Y., Fukui, T. & Aoki, H. Topological analysis of the quantum hall effect in graphene: Dirac-Fermi transition across van hove singularities and edge versus bulk quantum numbers. *Physical Review B* **74**, 205414 (2006).
27. Huo, S. Y., Chen, J. J., Huang, H. B. & Huang, G. L. Simultaneous multi-band valley-protected topological edge states of shear vertical wave in two-dimensional phononic crystals with veins. *Scientific Reports* **7**, 10335 (2017).
28. Yang, Y. H. *et al*. Observation of a topological nodal surface and its surface-state arcs in an artificial acoustic crystal. *Nature Communications* **10**, 5185 (2019).
29. Jia, D. *et al*. Acoustic topological insulator by honeycomb sonic crystals with direct and indirect band gaps. *New Journal of Physics* **20**, 093027 (2018).
30. Xia, J. P. *et al*. Programmable coding acoustic topological insulator. *Advanced Materials* **30**, 1805002 (2018).
31. Huang, X., Lai, Y., Hang, Z. H., Zheng, H. & Chan, C. T. Dirac cones induced by accidental degeneracy in photonic crystals and zero-refractive-index materials. *Nature Materials* **10**, 582–6 (2011).
32. Dai, H. Q., Xia, B. Z. & Yu, D. J. Dirac cones in two-dimensional acoustic metamaterials. *Journal of Applied Physics* **122**, 065103 (2017).
33. Chen, S. B., Wen, J. H., Wang, G., Yu, D. L. & Wen, X. S. Directionality of wave propagation and attenuation in plates with resonant shunting arrays. *Journal of Intelligent Material Systems and Structures* **27**, 28–38 (2016).
34. Wang, Y. Z., Li, F. M. & Wang, Y. S. Active feedback control of elastic wave metamaterials. *Journal of Intelligent Material Systems and Structures* **28**, 2110–2116 (2017).
35. Cardella, D., Celli, P. & Gonella, S. Manipulating waves by distilling frequencies: a tunable shunt-enabled rainbow trap. *Smart Materials and Structures* **25**, 085017 (2016).
36. Lossouarn, B., Deu, J. F. & Aucejo, M. Multimodal vibration damping of a beam with a periodic array of piezoelectric patches connected to a passive electrical network. *Smart Materials and Structures* **24**, 115037 (2015).
37. Manuel, C., Morvan, O. & Mohamed, N. I. Structural energy flow optimization through adaptive shunted piezoelectric metacomposites. *Journal of Intelligent Material Systems and Structures* **23**, 1661–1677 (2012).
38. Tateo, F., Collet, M., Quissen, M., Cunefare, K. & Abbe, P. Experimental characterization of a bi-dimensional array of negative capacitance piezo-patches for vibroacoustic control. *Journal of Intelligent Material Systems and Structures* **26**, 952–964 (2015).
39. Casadei, F., Beck, B., Cunefare, K. A. & Ruzzene, M. Vibration control of plates through hybrid configurations of periodic piezoelectric shunts. *Journal of Intelligent Material Systems and Structures* **23**, 1169–1177 (2012).
40. Chen, Z. G. *et al*. Accidental degeneracy of double Dirac cones in a phononic crystal. *Scientific Reports* **4**, 4613 (2014).

Acknowledgements

The authors acknowledge the supports by the National Natural Science Foundation of China (Grant Nos. 11772039 and 11991031), the Joint Sino-German Research Project (Grant No. GZ 1355) and the German Research Foundation (DFG, Grant No. ZH 15/27-1) for this research work.

Author contributions

Guan-Hua Li performed the numerical simulation and experiment with the cooperation of Tian-Xue Ma. Yi-Ze Wang discussed the results and developed the experimental model. Yue-Sheng Wang presented the helpful suggestions about the underlying mechanism and participated in the revision of the manuscript. All authors contributed to the writing and editing of the manuscript.

Competing interests

The authors declare no competing interests.

Additional information

Supplementary information is available for this paper at https://doi.org/10.1038/s41598-020-66269-2.

Correspondence and requests for materials should be addressed to Y.-Z.W.

Reprints and permissions information is available at www.nature.com/reprints.